A force balance model for the motion, impact, and bounce of bubbles

Klaseboer, Evert; Manica, Rogerio; Hendrix, Maurice H. W.; Ohl, Claus-Dieter; Chan, Derek Y. C.

2014

Klaseboer, E., Manica, R., Hendrix, M. H. W., Ohl, C.-D., & Chan, D. Y. C. (2014). A force balance model for the motion, impact, and bounce of bubbles. Physics of fluids, 26(9), 092101-.

https://hdl.handle.net/10356/107182

https://doi.org/10.1063/1.4894067

A force balance model for the motion, impact, and bounce of bubbles

Evert Klaseboer, Rogerio Manica, Maurice H. W. Hendrix, Claus-Dieter Ohl, and Derek Y. C. Chan

Citation: Physics of Fluids (1994-present) **26**, 092101 (2014); doi: 10.1063/1.4894067
View online: http://dx.doi.org/10.1063/1.4894067
View Table of Contents: http://scitation.aip.org/content/aip/journal/pof2/26/9?ver=pdfcov
Published by the AIP Publishing

PHYSICS OF FLUIDS **26**, 092101 (2014)

A force balance model for the motion, impact, and bounce of bubbles

Evert Klaseboer,[1] Rogerio Manica,[1,a)] Maurice H. W. Hendrix,[2] Claus-Dieter Ohl,[3] and Derek Y. C. Chan[4]
[1]*Institute of High Performance Computing, 1 Fusionopolis Way, Singapore 138632*
[2]*Laboratory for Aero and Hydrodynamics, Delft University of Technology, Leeghwaterstraat 21, NL-2628 CA Delft, The Netherlands*
[3]*School of Physical and Mathematical Sciences, Nanyang Technological University, Singapore 637371*
[4]*Department of Mathematics and Statistics, The University of Melbourne, VIC 3010, Australia and Department of Chemistry and Biotechnology, Swinburne University of Technology, Hawthorn 3122, Australia*

(Received 2 April 2014; accepted 8 August 2014; published online 3 September 2014)

A force balance model has been developed to predict the terminal velocity of a sub-millimetric bubble as its rises in water under buoyancy. The dynamics of repeated collisions and rebounds of the bubble against a horizontal solid surface is modeled quantitatively by including forces due to buoyancy, added mass, drag, and hydrodynamic lubrication—the last arises from the drainage of water trapped in the thin film between the solid surface and the surface of the deformable bubble. The result is a self-contained, parameter-free model that is capable of giving quantitative agreement with measured trajectories and observed collisions and rebounds against a solid surface as well as the spatio-temporal evolution of the thin film during collision as measured by interferometry. © *2014 AIP Publishing LLC*. [http://dx.doi.org/10.1063/1.4894067]

I. INTRODUCTION

To develop a unified model to describe a bubble rising under buoyancy and its subsequent collision with a horizontal solid surface that causes it to deform and rebound is a challenging task in fluid mechanics. For bubbles in the size range that are used in waste-water treatment, oil recovery, and mineral flotation[1–3] the fluid mechanics can vary from the small-Reynolds-number Stokes flow regime to intermediate and large Reynolds numbers. One characteristic length scale of the problem is the size of the bubble ∼1 mm. However, the interaction between the bubble and the horizontal solid surface requires a detailed description of the dynamics of the drainage of the fluid trapped between the solid surface and the surface of the bubble that may also deform as a result of the collision. Accurate quantification of the drainage process requires the film thickness and the local deformation of the bubble surface to be resolved to a scale 1000 times smaller, in the micrometer regime.

Investigations of the dynamics of bubble-solid interactions tend to fall into two broad classes:

(i) Studies that focus on determining the trajectory of the bubble and its collision by high speed video recordings[4–7] which may then describe the bubble dynamics in term of its center-of-mass. In particular, collisions of the bubble at a rigid solid-fluid and at deformable fluid-gas interfaces have been reported. The Navier-Stokes equation appropriate to such experiments has not been solved but the bubble has been treated as a "particle" with an effective mass.[8,9] The collision and rebound phenomenon are parameterized in terms of a coefficient of restitution. The value

[a)]Author to whom correspondence should be addressed. Electronic mail: manicar@ihpc.a-star.edu.sg

of this coefficient is not known *a priori*, but can be chosen to ensure good fit between theoretical predictions and experimental observations.

(ii) Investigations that record the spatio-temporal variations of the optical interference fringes generated between the solid-fluid and bubble-fluid interface from which the evolution of the shape of the trapped fluid can be extracted.[10–12] These experiments focus on the dynamics of the film drainage process as a bubble comes into near contact with the solid surface. Although models have been developed to treat the film drainage and associated bubble deformation processes in quantitative detail, information about the velocity of the bubble outside the film is needed as boundary conditions.[13–15] Such boundary conditions are taken from experimental measurements without any attempt to predict the trajectories of the bubbles.

Recently, through advances in high-speed video recording at up to 54 000 frames/s using synchronized cameras, the position of the bubble and the evolution of the interference fringes can be captured simultaneously. The latter allows measurements of the film thickness with sub-micrometer precision.[13]

In this paper, we propose a force balance model to describe the rising trajectory of a bubble and its collision with a horizontal solid surface. It is an extension of an earlier model by Klaseboer *et al.*[16] that included explicit descriptions of forces acting on the bubble. Although this model performed reasonably well when compared with the experimental center-of-mass collision and bounce data of Tsao and Koch,[4] no experimental information about the film thickness was available. This model was revisited recently by Kamran and Carnie.[17]

Although the model in Klaseboer *et al.*[16] included effects of bubble deformation and drainage of the thin fluid film between the bubble and the surface, this treatment, via lubrication theory, required setting the far field radius of the film to be about 30% larger than the bubble radius. This is needed to ensure the magnitude and phase of the rebound trajectory of the bubble is comparable to that observed experimentally. Beyond this there is no *a priori* justification for such a large asymptotic radius. Another feature omitted in previous models of bubble collision is the account of variation of the bubble's effective mass as a function of separation from the solid surface. As we shall see, this feature is responsible for the initial deceleration of the bubble as it approaches the surface, but before lubrication forces become significant.

To test our model, we provide a detailed comparison with experimental results that have been obtained for the time variations of the bubble trajectory as well as for the spatio-temporal variations of the thickness of the thin film of water trapped between the surface and the deforming bubble. Such comparisons with experimental data collected on two very different length scales (millimeter vs micrometer) constitute a more stringent test of the performance of the model.

II. FORCE BALANCE MODEL

Figure 1 depicts a schematic representation of the experiment and defines key variables of the model. Far from the solid surface a spherical bubble with radius R rises under buoyancy. We follow the time dependent trajectory of the center of mass of the bubble located at $z = b(t)$ that approaches the surface with instantaneous velocity, $V(t) = -db(t)/dt$, defined to be positive if the bubble is moving towards the solid surface. The coordinate z is directed positive downwards along unit vector $\mathbf{k}$ from the horizontal surface.

We now consider the various forces that control the rise of the bubble and its collision with the solid surface.

A. Buoyancy force

The buoyancy force that drives bubble rise in a fluid of density, ρ, has the form

$$\mathbf{F}_b = -\frac{4}{3}\pi R^3(\rho - \rho_b)g\,\mathbf{k} \quad \text{Buoyancy}, \tag{1}$$

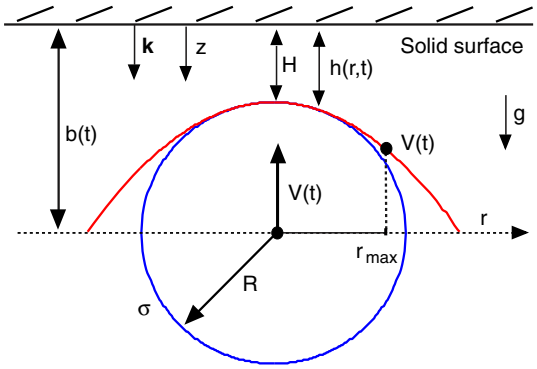

FIG. 1. Schematic representation of the bubble-surface experiment. The trajectory of the deformable bubble of radius R is defined in terms of the position of the center of mass at $z = b(t)$, and instantaneous velocity, $V(t) = -db(t)/dt$. The size of the computational domain in modeling film drainage is taken to be: $0 \le r < r_{\max} = 0.9\,R$.

where g is the acceleration due to gravity. The density of the bubble, ρ_b can be neglected since $\rho_b/\rho \sim 0.001$.

B. Drag force

When the bubble has attained its terminal rise velocity, the buoyancy force will be balanced by a hydrodynamic drag force. Unless the experiments are conducted in ultra pure water,[18–20] trace impurities in the water will render the hydrodynamic boundary condition on the bubble surface to be tangentially immobile.[21–24] This condition is the same as that on a rigid solid sphere. Thus the hydrodynamic drag force has the form

$$\mathbf{F}_d = \frac{\pi}{4} C_d\, Re\, \mu\, R\, V \quad \mathbf{k} \quad \text{drag force}, \tag{2}$$

where the drag coefficient, $C_{\rm d}$, can be estimated from the empirical Schiller and Naumann formula for a solid sphere[25,26]

$$C_d = (24/Re)(1 + 0.15\ Re^{0.687}) \quad \text{Schiller and Naumann drag coefficient} \tag{3}$$

with good accuracy for Reynolds numbers ($Re = 2R\rho|V|/\mu$) up to 800 for spheres. The use of Eqs. (1)–(3) gives very good agreement with the observed approach velocities of the bubbles considered in this paper where the experimental Reynolds number $Re \le 200$.[13–15]

C. Inertial (added mass) force

The inertia of the fluid surrounding an accelerating bubble is characterized by an added mass.[27] For a bubble of constant size in an infinite fluid medium, the associated inertial force has the form

$$\mathbf{F}_p^{\infty} = \frac{4\pi}{3}\ \rho\ R^3\ C_m(\infty)\ \frac{dV(t)}{dt} \quad \mathbf{k}, \tag{4}$$

where the added mass coefficient, $C_m(\infty) = 1/2$ for a sphere. However, as the bubble approaches the flat solid surface the effective mass increases due to the presence of the surface and the inertial force has the form:[28–30]

$$\mathbf{F}_p = \frac{4\pi}{3}\ \rho\ R^3\ \left(C_m(b)\ \frac{dV(t)}{dt}\ -\frac{1}{2}V^2(t)\frac{dC_m(b)}{db}\right) \quad \mathbf{k} \quad \text{Inertial added mass.} \tag{5}$$

This result is obtained from potential flow theory for a spherical bubble. An approximate analytic form, with a relative error of less than 10^{-4}, for the variation of the added mass coefficient, $C_m(b)$,

with bubble position, b (see Figure 1)[30] is

$$C_m(b) = \frac{1}{2} + 0.19222\left(\frac{b}{R}\right)^{-3.019} + 0.06214\left(\frac{b}{R}\right)^{-8.331} + 0.0348\left(\frac{b}{R}\right)^{-24.65} + 0.0139\left(\frac{b}{R}\right)^{-120.7}. \quad (6)$$

This provides an accurate interpolation for the monotonic variation between the value of $C_m(b = \infty) = 1/2$ for a sphere far from the surface to $C_m(b = R) = 0.803$ when the sphere is in contact with the surface. Note that in Eq. (5), the quantity dC_m/db is negative and reflects that the variation of the effective mass coefficient of the bubble with separation from the solid surface appears as an effective repulsion between the bubble and the surface.

D. History force

When a sphere undergoes unsteady motion characterized by a time-varying velocity, $V(t)$, in an infinite fluid of dynamic shear viscosity, μ, the solution of the time dependent linearized Navier-Stokes equation results in a force on the sphere at time, t, that is dependent on the acceleration, dV/dt, at all times prior to t. This is known as the history or Basset force. For a sphere with a tangentially immobile boundary condition, the history force $\mathbf{F}_h(t)$ has the form:[31,32]

$$\mathbf{F}_h = 6\sqrt{\pi\mu\rho}\, R^2 \int_{-\infty}^{t} \frac{1}{\sqrt{t-\tau}} \frac{dV(\tau)}{d\tau}\, d\tau \quad \mathbf{k} \quad \text{History force.} \quad (7)$$

The assumption of the immobile boundary condition is consistent with the use of the Schiller and Naumann formula, Eq. (3), to describe the hydrodynamic drag that determines the bubble terminal velocity. On the other hand, if the sphere surface has a zero tangential stress boundary condition, the magnitude of the history force is considerably smaller.[32]

E. Thin film drainage and surface forces

The short-ranged interaction between the bubble and the flat surface during collision is determined by the lubrication drainage of the water trapped between the rigid surface and the deforming surface of the bubble. In addition, surface forces such as electrical double layer interaction and van der Waals forces between the surface and the bubble can also be important if the water film becomes sufficiently thin. An accurate, quantitative description of such interactions can be given in terms of the Stokes-Reynolds-Young-Laplace model.[33,34] If the deformation of the bubble surface during collision is taken to be axisymmetric, the local deformation of the instantaneous local film thickness, $h(r,t)$ is given by the Young-Laplace equation

$$\frac{\sigma}{r}\frac{\partial}{\partial r}\left(r\frac{\partial h(r,t)}{\partial r}\right) = \frac{2\sigma}{R_L} - \Pi(h(r,t)) - p(r,t) \quad \text{Young-Laplace,} \quad (8)$$

where σ is the surface tension of the bubble and the Laplace pressure of the bubble, $(2\sigma/R_L)$, defines the Laplace radius R_L. If the deformation of the bubble as a result of collision with the surface is small, R_L can be approximated by the radius of curvature of the bubble when it is far from the surface. Here it is taken to be R. The disjoining pressure $\Pi(h)$ accounts for electrical double layer and van der Waals interaction and $p(r,t)$ is the pressure. The evolution of the bubble in the thin film region is governed by the Stokes-Reynolds equation

$$\frac{\partial h(r,t)}{\partial t} = \frac{1}{12\mu r}\frac{\partial}{\partial r}\left(r\, h^3(r,t)\,\frac{\partial p(r,t)}{\partial r}\right) \quad \text{Stokes-Reynolds.} \quad (9)$$

The solution of Eqs. (8) and (9) gives the pressure distribution in the film from which the lubrication and short-ranged surface force between the surface and the bubble is found from

$$\mathbf{F}_f = \int_0^\infty 2\pi\ r\ p(r,t)\ dr \quad \mathbf{k} \quad \text{Film drainage.} \tag{10}$$

The numerical solution of Eqs. (8)–(10) for the Stokes-Reynolds-Young-Laplace model has been discussed in detail in the literature.[35]

III. THE BUBBLE EQUATION OF MOTION

The equation of motion of the bubble, neglecting the density of the bubble, $\rho_b = 0$, is obtained by balancing all the point forces (Secs. II A–II E) in Sec. II: $\mathbf{F}_b + \mathbf{F}_d + \mathbf{F}_p + \mathbf{F}_h + \mathbf{F}_f = \mathbf{0}$, or explicitly

$$\begin{aligned}
&-\frac{4}{3}\pi R^3 \rho g \quad \text{(Buoyancy)}\\
&+\frac{\pi}{4} C_d\, Re\, \mu\, R\, V \quad \text{(Schiller and Naumann drag)}\\
&+\frac{4\pi}{3}\ \rho\ R^3 \left(C_m \frac{dV(t)}{dt} - \frac{1}{2} V^2(t) \frac{dC_m}{db} \right) \quad \text{(Inertial/added mass)}\\
&+6\sqrt{\pi\mu\rho}\ R^2 \int_{-\infty}^{t} \frac{1}{\sqrt{t-\tau}} \frac{dV(\tau)}{d\tau}\, d\tau \quad \text{(History)}\\
&+\int_0^\infty 2\pi\ r\ p(r,t)\ dr \quad \text{(Film drainage)} = 0,
\end{aligned} \tag{11}$$

where the velocity-dependent drag coefficient, C_d, and the position-dependent added mass coefficient, C_m, are given by Eqs. (3) and (6), respectively.

As we will demonstrate in Sec. IV, although the model encapsulated by Eq. (11) will describe the experimental terminal velocities of the bubbles, there are inherent inconsistencies and hence possible limitations in its formulation. The inertial added mass term[28–30] is obtained under the assumption of a spherical bubble and inviscid potential flow. However, it appears that variations of the added mass coefficient are only important when the surface of the bubble is within about one radius of the solid surface. When the bubble is further away, the added mass coefficient is close to its value of 1/2 corresponding to a bubble in an infinite fluid. When the bubble surface is closer than about one radius to the surface, the lubrication force will start to dominate.

The second inconsistency in Eq. (11) is that the Reynolds number corresponding to the observed terminal velocities of the bubble can be as high as $Re \sim 200$ whereby the Schiller and Naumann expression for the drag force will be accurate. However, the expression for the history force is derived from the linearized time-dependent Stokes equation that is strictly applicable for $Re = 1$. In the absence of a better theory, we persevere with this approximation. With the benefits of hindsight obtained through comparison with experimental data (see Sec. IV) this approximation does not appear to give rise to significant error.

A final observation is related to the solution of the Stokes-Reynolds-Young-Laplace (SRYL) equations, (8) and (9). They account for the film drainage force in the deformation zone defined by $r \le r_{max}$, in which these two equations needed to be solved. In previous work[16] that focussed on modelling the bubble trajectory, the SRYL equations are solved in the domain $0 < r < r_{max}$, with $r_{max} = 1.3\ R$. Although this is an obviously unphysical domain to take, it is nonetheless a necessary assumption in order to obtain trajectories that are close to experimental observations. In our analysis, it turns out that the need for such an unphysically large domain is due to the omission in accounting for the variations of the added mass coefficient with separation between the bubble

and surface.[16] In our force balance model, solving the SRYL equation in the domain $0 < r < r_{max} = 0.9\,R$ provided good quantitative description of the experimental data for the bubble trajectories and for the evolution of the film profiles. The history force was evaluated without the approximation used in Refs. 17 and 36.

IV. COMPARISON WITH EXPERIMENTS

The experimental results of Hendrix *et al.*[13] consist of high speed video recordings of the position of rising bubbles of radius of around 500 μm and synchronized video recordings of the evolution of the interference fringe patterns between the horizontal glass-water interface and the bubble-water interface during bubble-surface collision. From the video recordings of the bubble position, the bubble velocity as a function of time, $V(t)$, is extracted. The evolution of the film thickness, $h(r,t)$, as a function of position and time can be obtained by analyzing the axisymmetric interference fringe patterns.[13–15]

Initially, as the bubble approaches the surface after attaining its terminal rise velocity, the minimum film thickness is located at the axis of symmetry, $r = 0$, since the bubble surface is still spherical. However, as film drainage progresses, the bubble surface deforms with axial symmetry. The characteristic dimple in the film then develops so that the position of minimum film thickness, $h_{\rm m}$ will then be relocated to $r = r_m$, commonly referred to as the film barrier rim. The value of r_m also varies as the bubble approaches closer to the surface.

As the bubble approaches the solid planar surface, it starts to decelerate and eventually comes to a halt. It then reverses direction and rebounds to move away from the surface until buoyancy force drives the bubble back towards the surface again. This bubble-surface encounter is a series of rebounds with decreasing amplitude until the bubble settles with a thin draining film separating it from the surface. After a period much longer than the rebound period, the film eventually ruptures.

In Figure 2 we compare the time evolution of the experimental and predicted bubble position, $b(t)$ and velocity, $V(t)$; the characteristic film thicknesses at the axis of symmetry: $h_o(t) \equiv h(r = 0,t)$ and at the barrier rim (when it exists) where the film thickness is a minimum: $h_m(t) \equiv h(r_m,t)$; and the magnitudes of various forces in Eq. (11) that act on the bubble. In Figures 2(a)–2(c), we show these results for a bubble with radius, $R = 385$ μm and in Figures 2(d)–2(f), we show the same results for a bubble of radius, $R = 630$ μm. The time axes of each of the 3 figures are aligned to the same arbitrary reference $t = 0$, to indicate the relative chronology of the bubble trajectory, film thickness evolution, and the relative magnitude of the various forces in Eq. (11) at different stages of the bubble-surface encounter.

Note that different scales are used on different parts of the time axes. For the $R = 630$ μm bubble, the film between the solid surface and the bubble ruptured at $t = 255$ ms whereas for the smaller $R = 385$ μm bubble, the video recordings terminated at 180 ms when the film is still intact.

The following observations can be made concerning the results in Figure 2:

(a) The force balance model given by Eq. (11) provides quantitatively accurate predictions of the time variations of the position and velocity of bubble rise and subsequent collisions and rebounds against the solid surface.

(b) Surface forces that contribute to the disjoining pressure $\Pi(h)$ in the Young-Laplace equation (8) have not been included in the present model. The film rupture observed for the $R = 630$ μm bubble in Figures 2(d) and 2(e), occurring at minimum film thickness of $h_m \sim 0.5$ μm, is due to the bubble being punctured by asperities on the solid or triggered by the presence of hydrophobic contaminants as surface forces relevant to this system are small for ideally smooth surfaces at this separation. A more precise cause for the rupture of the water film that is <1 μm thick will require more detailed surface chemical analysis.

(c) The force balance model is the least accurate when the bubble is about one radius from the surface. At this separation, the most important forces are the inertial added mass force, Eq. (5) and the history force, Eq. (7). From the discussion at the end of Sec. III, we recognize that the assumptions that underpin the force balance model are likely to be less precise when the bubble is about one radius from the sphere.

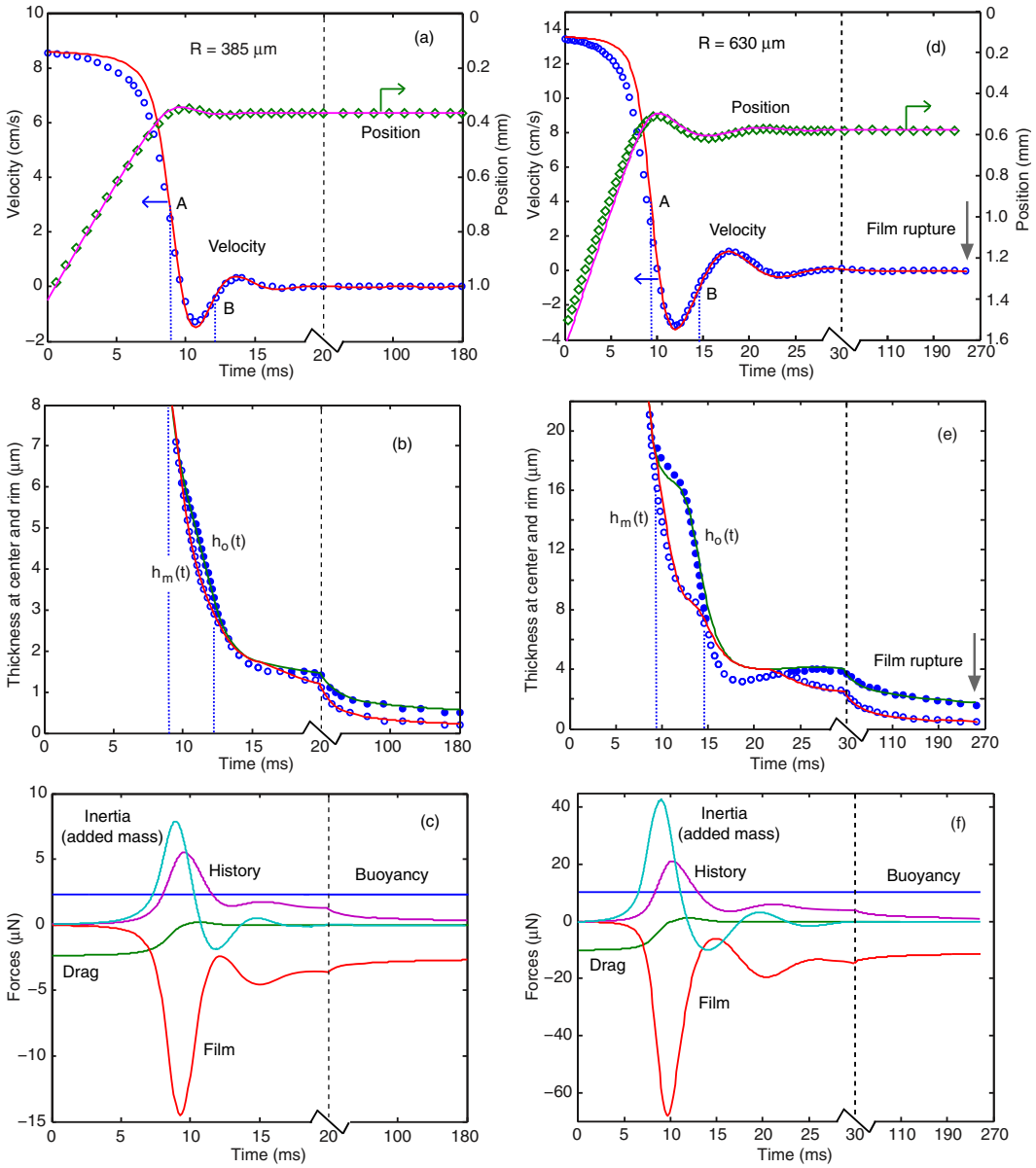

FIG. 2. A comparison of experimental (symbols) and force balance model predictions (lines) of the time variations of center of mass positions and velocities of rising bubbles colliding with a horizontal solid surface, the film thickness at the center $h_o(t)$, and at the barrier rim $h_m(t)$ of the bubble as well as the force components of the model at different times. (a)–(c) Results for a bubble of radius $R = 385$ μm and (d)–(f) for a bubble with $R = 630$ μm. The points marked "A" and "B" correspond to the first and last line in Figure 3 where film profiles during the first impact are shown.

(d) The dimpling phenomena, observed as the bifurcation of the film thickness into $h_o(t)$ and $h_m(t)$ as well as the rebound positions and velocities are predicted quite accurately by the model. This highlights the important role of the history force, Eq. (7) and the film drainage force, Eq. (10) that are the dominant terms in the force balance model in the bubble bouncing regime at times $t \geq 10$ ms. See Figures 2(c) and 2(f) and Sec. V for further discussions.

(e) In our model, the simple addition of the Schiller-Naumann drag force given by Eq. (2) and the lubrication force given by Eq. (10) has in theory counted the pressure contribution from the front part of the bubble twice. However, as can be seen in Figures 2(c) and 2(f), the magnitude of the Schiller-Naumann drag force is significant when the bubble is far from the solid surface where the bubble velocity is high. In the same regime, the lubrication force is

negligible. As the bubble approaches the surface and slows down, the Schiller-Naumann drag force decreases rapidly and contemporaneously the magnitude of lubrication force increases rapidly as the bubble-surface separation decreases. Thus the "double counting" only occurs over a small separation or time interval.

(f) The experimentally observed terminal velocity of ∼13 cm/s for the 630 μm radius bubble is consistent with the tangentially immobile hydrodynamic boundary condition at the bubble surface, like that on a solid sphere. This value for the terminal velocity is consistent with the prediction from the Schiller-Naumann formula. In contrast, for bubbles of the same size in ultra clean water obeying the tangentially mobile boundary condition, the terminal velocity is expected to be ∼32 cm/s.[18,19] The experimental reason for the difference is that the water in the experiments we considered was open to the laboratory atmosphere and that is sufficient for trace impurities to be adsorbed on the bubble surface to change the nature of the boundary condition.

In Figure 3, we compare the experimental film profile deduced from interferometry data and predictions of the force balance model during the first approach of the bubble to the surface in between the time marked by "A" and "B" in Figure 2. There is also good quantitative agreement in the observed and predicted film profiles in Figures 3(a) and 3(b). The hydrodynamic pressure, $p(r,t)$, profiles that contribute to the film drainage force in the same time interval are shown in Figures 3(c) and 3(d). We see that when the pressure exceeds the Laplace pressure, $2\sigma/R$, of the bubble, the film dimple develops with the minimum thickness, h_m, of the film located at the barrier rim, r_m, rather than at the center of the film at $r = 0$. As the bubble retracts from the surface, between

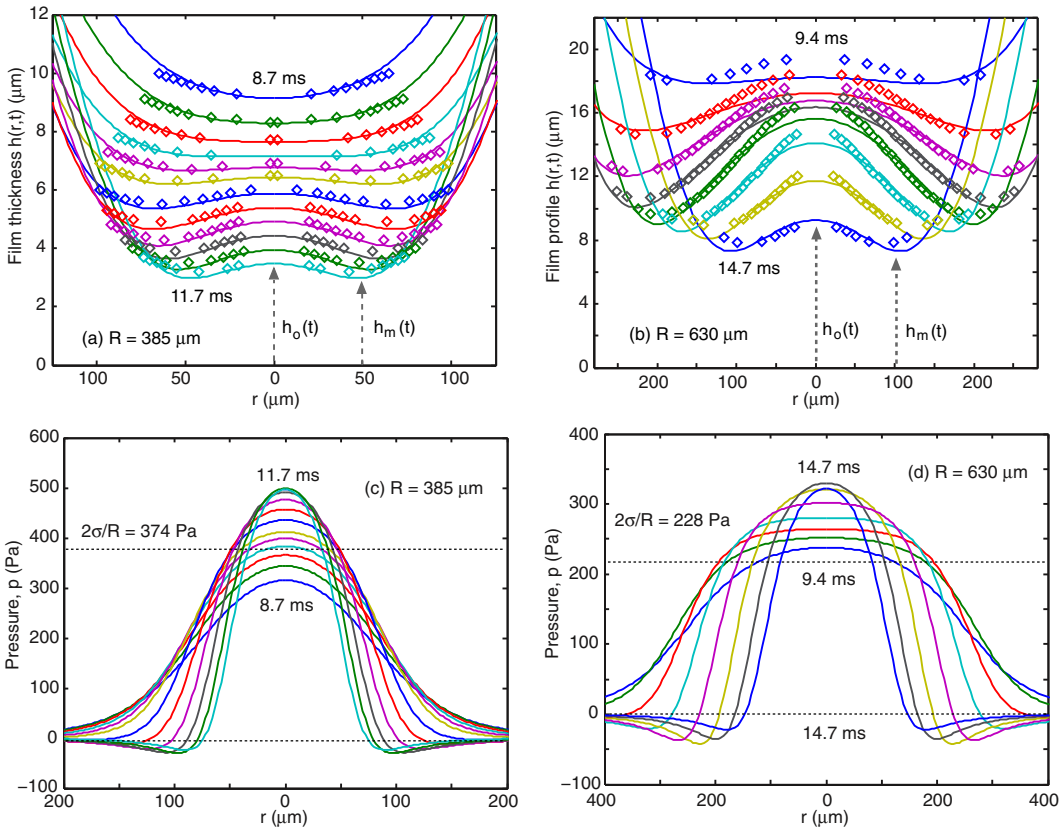

FIG. 3. Comparison of experimental (symbols) and force balance model predictions (lines) of the film profile for the (a) $R = 385$ μm and (b) $R = 630$ μm bubble during the initial approach indicated between the points marked "A" and "B" in Figure 2. The corresponding pressure profiles are shown in (c) and (d) relative to the Laplace pressure of each bubble: $2\sigma/R$.

12 and 18 ms in each case, the pressure becomes negative around the barrier rim, signifying an attractive hydrodynamic contribution that opposes the separation of the bubble from the surface.

V. DISCUSSION AND CONCLUSIONS

It is instructive to quantify in more detail the effect of the history force and the variable added mass of the bubble on the bubble velocity and on the film profiles. In Figure 4, we compare the effects on the bubble velocity when either the history force is omitted or when the separation variation of the effective mass coefficient, C_m, is omitted, that is, assumed to have the constant value $C_m = 1/2$. In these comparisons, all other model parameters are kept constant.

In Figure 4(a) we can see that the failure to account for the effective mass, C_m increasing from 0.5 to 0.8 as the bubble approaches the surface means that the bubble velocity becomes too high because the increase in inertia has been omitted. On the other hand, with the omission of the history force that helps the bubble "remember" how fast it has been travelling in the past, the approach velocity becomes lower. However, since the model in Eq. (11) has inherent approximations in the history force and the variation of C_m with separation, it still overestimates the magnitude of the bubble velocity on approach to the surface.

The effect of omitting the history force is quite marked in affecting the magnitude and period of the bubble rebound velocity as shown in Figure 4(b). During this rebound phase, the magnitude of the velocity is small and therefore the history force obtained from the linearized Stokes equation should become more accurate. Thus the use of a mathematically incorrect simplification[17,36] to treat the history force is not recommended.

Consistent with the above observation, we see in Figure 5(a) that omission of the history force results in large errors in the predicted film thickness at the center of the film: $h_o(t) = h(r = 0,t)$, and at the barrier rim: $h_m(t) = h(r = r_m,t)$. The assumption that the effective mass coefficient is constant: $C_m = 1/2$ has a less marked effect on the film profiles seen in Figures 5(a) and 5(b) in that the onset of dimple development and the height of the dimple are quantitatively different from the experiment.

In the original model of Klaseboer *et al.*,[16] the effective mass coefficient was taken to be a constant, $C_m = 1/2$. We see in Figure 6 that this simplification can be compensated by choosing the size of the integration domain of the Stokes-Reynolds-Young-Laplace equation to be 1.5 times the bubble radius: $r_{max} = 1.5\,R$. Although such a choice does not have a sound physical basis, it can actually produce quite a good fit to the measured bubble velocity (Figure 6(a)). However, the predictions of the characteristic film thickness $h_o(t) = h(r = 0,t)$ and $h_m(t) = h(r = r_m,t)$ are not as good as the present model in Eq. (11) (Figure 6(b) and cf. Figure 5(a)). Physically, we must have $r_{max} \leq R$ and the choice $r_{max} = 0.9\,R$ provided good agreement with experimental data and the difference

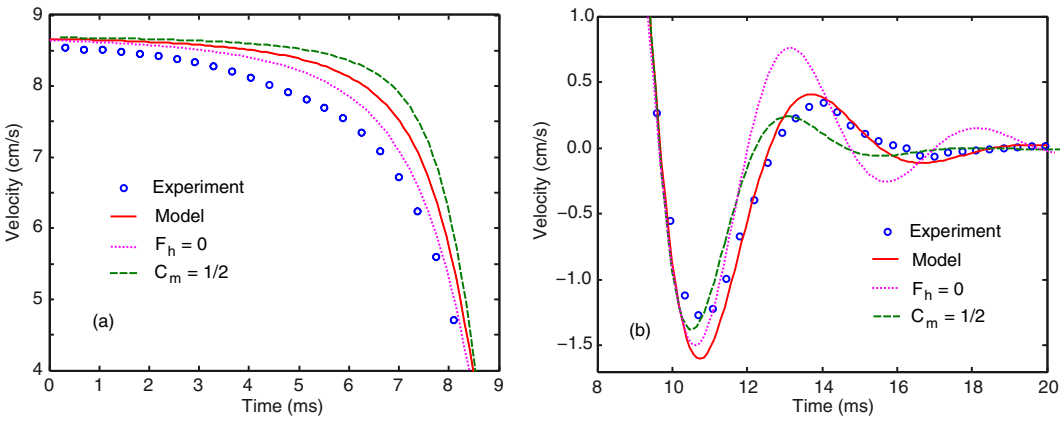

FIG. 4. A comparison of effects on the bubble velocity, $V(t)$, as a result of omitting the history force, F_h, or the separation dependence of the added mass coefficient, C_m, during (a) the approach phase and (b) the bounce phase of the bubble: o o o (blue): experimental data, —— (red): present model according to Eq. (11), ... (pink): omitting the history force, and - - - (green): using a constant added mass coefficient, $C_m = 1/2$.

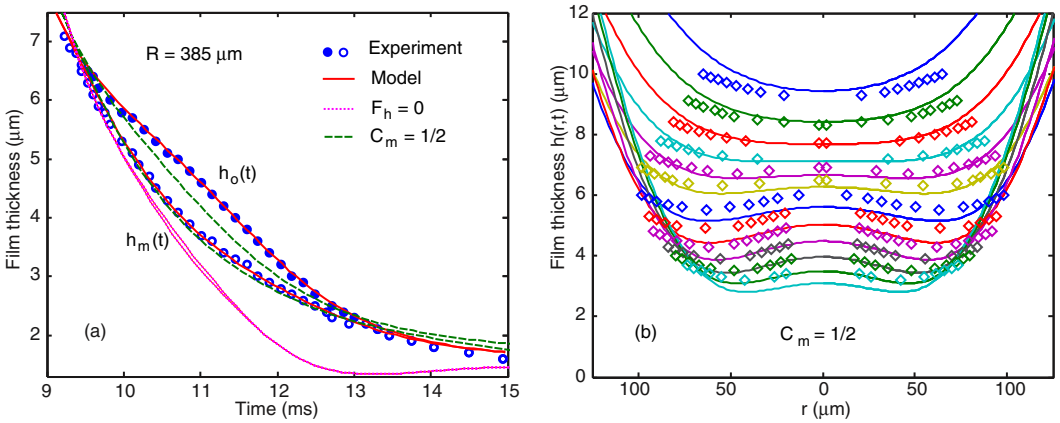

FIG. 5. A comparison of effects of omitting the history force, F_h, or the separation dependence of the added mass coefficient, C_m, on (a) the center of the film, $h_o(t) = h(r = 0,t)$ and the film thickness at the barrier rim, $h_m(t) = h(r = r_m,t)$: o o o (blue): experimental data, —— (red): present model according to Eq. (11), **. . . .** (pink): omitting the history force, and **- - -** (green): using a constant added mass coefficient, $C_m = 1/2$, and (b) the film profile, $h(r,t)$: symbols are experimental data, and lines are predictions using a constant added mass coefficient, $C_m = 1/2$.

between the asymptotic parabolic shape of the water film is still close to the actual surface of the spherical bubble, see Figure 1.

In our model, the variation of the added mass of the bubble with separation from the flat solid surface was taken to be the form given by a sphere under inviscid potential flow. Also, we have only employed the Basset expression, Eq. (7), as history force. We note from Figures 2(c) and 2(f) that this force is important only in the transition regime when the bubble first became close to the surface as it decelerates rapidly from the terminal velocity. Thereafter, it is the buoyancy force and the lubrication force that play the dominant role in determining the bubble trajectory. Although a more complex expression for the history is available,[37] the limited role of the history force probably justifies the use of the simple Basset expression.

We have constructed a force balance model to analyze the rise and collision of a bubble with a solid surface that can account quantitatively for phenomena on the scale of the bubble size (∼1 mm) and on a much smaller scale of the film drainage and bubble deformation (∼1 μm). In Figures 2(c) and 2(f), we see that on approaching the surface the drag force (a bubble size ∼1 mm phenomenon) is large, whereas the film drainage force (a film size ∼1 μm phenomenon) is small. But during bubble

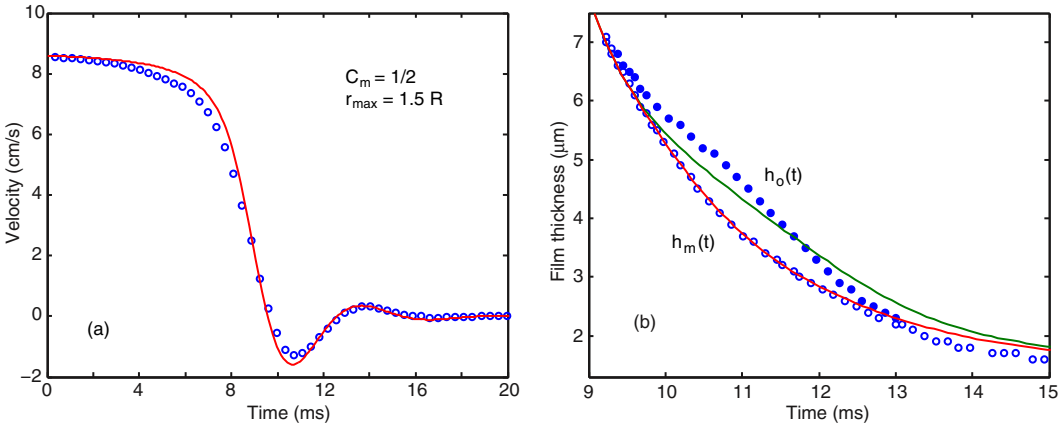

FIG. 6. A demonstration of compensating the use of a constant effective mass coefficient, $C_m = 1/2$ with increasing the size of the integration domain of the Stokes-Reynolds-Young-Laplace equation to $r_{max} = 1.5\ R$. (a) Bubble velocity and (b) film thickness at the center and at the rim.

collision and rebound, when the bubble velocity is small, the drag force is unimportant whereas the film drainage and bubble deformation are dominant. Although the model contains obvious and necessary simplifications, it is successful in capturing the main physics of the problem and handling the transition of phenomena on very different length scales. There is potential to extend the current approach to model bubble-wall experiments that study oblique collisions and bubble sliding motion along the wall.[38,39] It can also serve as a useful complement to full-scale direct numerical simulation approaches that may find it challenging to have to resolve physical processes accurately over such a large range of length scales.

ACKNOWLEDGMENTS

This work is supported in part by an Australian Research Council Discovery Project Grant to D.Y.C.C. who is a Visiting Scientist at the Institute of High Performance Computing when part of this work was carried out.

[1] N. Liu, Q. Zhang, G.-L. Chin, E.-H. Ong, J. Lou, C.-W. Kang, W. Liu, and E. Jordan, "Experimental investigation of hydrodynamic behavior in a real membrane bio-reactor unit," J. Membr. Sci. **353**, 122 (2010).
[2] A. C. Bannwart, O. M. H. Rodriguez, F. E. Trevisan, F. F. Vieira, and C. H. M. de Carvalho, "Experimental investigation on liquid-liquid-gas flow: Flow patterns and pressure-gradient," J. Pet. Sci. Eng. **65**, 1 (2009).
[3] A. M. Kamp, C. Heny, L. Andarcia, M. Lago, and A. Rodriguez, "Experimental investigation of foamy oil solution gas drive," paper presented at the SPE International Thermal Operations and Heavy Oil Symposium, Porlamar, Margarita Island, Venezuela, 2001.
[4] H. K. Tsao, and D. L. Koch, "Observations of high Reynolds number bubbles interacting with a rigid wall," Phys. Fluids **9**, 44 (1997).
[5] K. Malysa, M. Krasowska, and M. Krzan, "Influence of surface active substances on bubble motion and collision with various interfaces," Adv. Colloid Interface Sci. **114**, 205 (2005).
[6] F. Suñol, and R. González-Cinca, "Rise, bouncing and coalescence of bubbles impacting at a free surface," Colloids Surf. A: Physicochem. Eng. Aspects **365**, 36 (2010).
[7] D. Kosior, J. Zawala, and K. Malysa, "Influence of n-octanol on the bubble impact velocity, bouncing and the three-phase contact formation at hydrophobic solid surfaces," Colloids Surf. A: Physicochem. Eng. Aspects **441**, 788 (2014).
[8] R. Zenit and D. Legendre, "The coefficient of restitution for air bubbles colliding against solid walls in viscous liquids," Phys. Fluids **21**, 083306 (2009).
[9] D. Legendre, R. Zenit, and J. R. Velez-Cordero, "On the deformation of gas bubbles in liquids," Phys. Fluids **24**, 043303 (2012).
[10] B. V. Derjaguin and M. Kussakov, "Anomalous properties of thin polymolecular films," Acta Physicochim. URSS **10**, 26 (1939); Prog. Surface Sci. **40**, 26 (1992) (Reprinted).
[11] A. Sheludko, "Thin liquid films," Adv. Colloid Interface Sci. **1**, 391 (1967).
[12] L. R. Fisher, D. Hewitt, E. E. Mitchell, J. Ralston, and J. Wolfe, "The drainage of an aqueous film between a solid plane and an air bubble," Adv. Colloid Interface Sci. **39**, 397 (1992).
[13] M. H. W. Hendrix, R. Manica, E. Klaseboer, D. Y. C. Chan, and C.-D. Ohl, "Spatiotemporal evolution of thin liquid films during impact of water bubbles on glass on a micrometer to nanometer scale," Phys. Rev. Lett. **108**, 247803 (2012).
[14] R. Manica, M. H. W. Hendrix, R. Gupta, E. Klaseboer, C.-D. Ohl, and D. Y. C. Chan, "Effects of hydrodynamic film boundary conditions on bubble-wall impact," Soft Matter **9**, 9755 (2013).
[15] R. Manica, M. H. W. Hendrix, R. Gupta, E. Klaseboer, C-D. Ohl, and D. Y. C. Chan, "Modelling bubble rise and interaction with a glass surface," Appl. Math. Model. **38**, 4249–4261 (2014).
[16] E. Klaseboer, J.-P. Chevaillier, A. Maté, O. Masbernat, and C. Gourdon, "Model and experiments of a drop impinging on an immersed wall," Phys. Fluids **13**, 45 (2001).
[17] K. Kamran and S. L. Carnie, "Modeling the gentle bouncing of a drop with quasi-static thin film equations," Chem. Eng. Sci. **104**, 361 (2013).
[18] P. C. Duineveld, "The rise velocity and shape of bubbles in pure water at high Reynolds number," J. Fluid Mech. **292**, 325 (1995).
[19] J. Zawala and K. Malysa, "Influence of the impact velocity and size of the film formed on bubble coalescence time at water surface," Langmuir **27**, 2250 (2011).
[20] L. Parkinson, R. Sedev, D. Fornasiero, and J. Ralston, "The terminal rise velocity of 10-100 μm diameter bubbles in water," J. Colloid Interface Sci. **322**, 168 (2008).
[21] R. Bel Fdhila and P. C. Duineveld, "The effect of surfactant on the rise of a spherical bubble at high Reynolds and Peclet numbers," Phys. Fluids **8**, 310 (1996).
[22] G. H. Kelsall, S. Tang, A. L. Smith, and S. Yurdakul, "Electrophoretic behaviour of bubbles in aqueous electrolytes," Faraday Trans. **92**, 3879 (1996).
[23] L. Parkinson, and J. Ralston, "Dynamic aspects of small bubble and hydrophilic solid encounters," Adv. Colloid Interface Sci. **168**, 198 (2011).
[24] R. Manica, L. Parkinson, J. Ralston, and D. Y. C. Chan, "Interpreting the dynamic interaction between a very small rising bubble and a hydrophilic titania surface," J. Phys. Chem. C **114**, 1942 (2010).
[25] L. Schiller and A. Naumann, "Über die grundlegenden berechnungen bei der schwerkraftaufbereitung," Zeit. Ver. Deut. Ing. **77**, 318 (1933).

[26] R. Clift, J. R. Grace, and M. E. Weber, *Bubbles, Drops and Particles* (Academic Press, NY, 1978).
[27] C. D. Ohl, A. Tijink, and A. Prosperetti, "The added mass of an expanding bubble," J. Fluid Mech. **482**, 271 (2003),
[28] H. Lamb, *Hydrodynamics* (Dover, New York, 1932).
[29] T. Miloh, "Hydrodynamics of deformable contiguous spherical shapes in an incompressible inviscid fluid," J. Eng. Math. **11**, 349 (1977).
[30] A. A. Kharlamov, Z. Chára, and P. Vlasák, "Hydraulic formulae for the added masses of an impermeable sphere moving near a plane wall," J. Eng. Math. **62**, 161 (2007).
[31] A. B. Basset, *A Treatise on Hydrodynamics with Numerous Examples* (Deighton, Bell and Co., Cambridge, 1888), Vol II, p. 285–286.
[32] S.-M. Yang, and L. G. Leal, "A note on memory-integral contributions to the force on an accelerating spherical drop at low Reynolds number," Phys. Fluids A **3**, 1822 (1991).
[33] D. Y. C. Chan, E. Klaseboer, and R. Manica, "Film drainage and coalescence between deformable drops and bubbles," Soft Matter **7**, 2235 (2011).
[34] E. Klaseboer, R. Gupta, and R. Manica "An extended Bretherton model for long Taylor bubbles at moderate capillary numbers," Phys. Fluids **26**, 032107 (2014).
[35] D. Y. C. Chan, E. Klaseboer, and R. Manica, "Theory of non-equilibrium force measurements involving deformable drops and bubbles," Adv. Colloid Interface Sci. **165**, 70 (2011).
[36] R. I. Nigmatulin, *Dynamics of Multiphase Media* (Hemisphere, New York, 1990), Vol. 1.
[37] R. Mei and R. J. Adrian, "Flow past a sphere with an oscillation in the free-stream velocity and unsteady drag at finite Reynolds number," J. Fluid Mech. **237**, 323 (1992).
[38] L. A. Del Castillo, S. Ohnishi, and R. G. Horn, "Inhibition of bubble coalescence: Effects of salt concentration and speed of approach," J. Colloid Interface Sci. **356**, 316 (2011).
[39] L. A. Del Castillo, S. Ohnishi, L. R. White, S. L. Carnie, and R. G. Horn, "Effect of disjoining pressure on terminal velocity of a bubble sliding along an inclined wall," J. Colloid Interface Sci. **364**, 505 (2011).